

# Enhancing Solutions for Complex PDEs: Introducing Complementary Convolution and Equivariant Attention in Fourier Neural Operators

Xuanle Zhao<sup>1,2\*</sup>, Yue Sun<sup>1\*</sup>, Tielin Zhang<sup>1,2</sup>, Bo Xu<sup>1,2</sup>

<sup>1</sup>Institute of Automation, Chinese Academy of Sciences

<sup>2</sup>School of Artificial Intelligence, University of Chinese Academy of Sciences

## Abstract

Neural operators improve conventional neural networks by expanding their capabilities of functional mappings between different function spaces to solve partial differential equations (PDEs). One of the most notable methods is the Fourier Neural Operator (FNO), which draws inspiration from Green's function method and directly approximates operator kernels in the frequency domain. However, after empirical observation followed by theoretical validation, we demonstrate that the FNO approximates kernels primarily in a relatively low-frequency domain. This suggests a limited capability in solving complex PDEs, particularly those characterized by rapid coefficient changes and oscillations in the solution space. Such cases are crucial in specific scenarios, like atmospheric convection and ocean circulation. To address this challenge, inspired by the translation equivariant of the convolution kernel, we propose a novel hierarchical Fourier neural operator along with convolution-residual layers and attention mechanisms to make them complementary in the frequency domain to solve complex PDEs. We perform experiments on forward and reverse problems of multiscale elliptic equations, Navier-Stokes equations, and other physical scenarios, and find that the proposed method achieves superior performance in these PDE benchmarks, especially for equations characterized by rapid coefficient variations.

## Introduction

Conventional research in the deep learning field is predominantly driven by neural networks designed to learn relationships between input and output pairs that lie in finite-dimensional spaces. These designs have led to notable breakthroughs in numerous domains, including computer vision (He et al. 2016; Chen et al. 2018), natural language processing (Zhou et al. 2016; Devlin et al. 2018), reinforcement learning (Hafner et al. 2019), and signal processing (Dong, Xu, and Xu 2018; Gulati et al. 2020).

Partial differential equations (PDEs) are utilized in scientific research to describe a wide variety of physical, chemical, and biological phenomena (Sommerfeld 1949; Zhang et al. 2023). From turbulent flows to atmospheric circulation and material stress analysis, numerous real-world phenomena are fundamentally governed by the underlying PDEs. Therefore, solving PDEs is a crucial aspect of addressing problems in natural science.

\*These authors contributed equally.

Traditional numerical methods for solving PDEs, such as the finite element method (FEM) and the finite difference method (FDM), present challenges in terms of incorporating noisy data, generating complex meshes, solving high-dimensional problems, and handling inverse problems. Fortunately, by harnessing the expressiveness of neural networks, many innovative methods (Hao et al. 2023; Brandstetter et al. 2022; Liu et al. 2023; Li, Meidani, and Farihani 2022; Zhao et al. 2024b) have been proposed to effectively overcome the limitations of numerical methods in solving PDEs. Examples of such methods include physics-informed neural networks (PINN) (Karniadakis et al. 2021) and Galerkin transformers (GT) (Cao 2021), which are specifically designed neural networks for PDE simulation by estimating the mapping between inputs and output pairs. In addition, methods such as the deep operator network (DeepONet) (Lu, Jin, and Karniadakis 2019) and the Fourier Neural Operator (FNO) (Li et al. 2020, 2022) attempt to learn an operator between input and output function spaces. Besides solving PDEs, these methods have also proven to be effective in dealing with issues related to complex dynamics such as climate change and natural disasters (Gopakumar et al. 2023; Pathak et al. 2022; Zhao et al. 2024a).

We preferentially consider more complex PDEs, such as multiscale PDEs, which have been widely used in physics, engineering, and related disciplines for analyzing complex practical problems such as reservoir modeling, ocean circulation, and high-frequency scattering (Quarteroni and Veneziani 2003). Given that complex PDEs are characterized by rapidly changing coefficients and oscillations in the solution space, it is crucial to capture information across various scales and frequency ranges. Nevertheless, when applied to solving PDEs, evidence shows that FNO and related methods tend to prioritize learning low-frequency components (Li et al. 2020; Liu, Xu, and Zhang 2022; Anonymous 2023), which raises the key question about how to capture high-frequency features and combine them with low-frequency features of the FNO for solving complex PDEs.

In this paper, we presented a novel attentive hierarchical FNO method that attempts to capture and integrate low-frequency and high-frequency features at different scales. Since the convolution kernel is locally computed, high-frequency local details can be captured efficiently. Therefore, inspired by DCNO (Anonymous 2023), we adopt the

Fourier kernel with the convolutional-residual layer, which aims to improve the ability to capture high-frequency information. Furthermore, we theoretically prove that the attention mechanism composed of channel and spatial attention could integrate before the Fourier layer in a translation equivariant way. Furthermore, to effectively capture information across different scales, we propose a hierarchical architecture that learns convolutional-residual Fourier layers and equivariant attentions at multiple scales. Our main contributions can be summarized as follows:

- We propose an enhanced method to address the issue where FNO-related approaches struggle to capture high-frequency features effectively. Specifically, our method integrates high-frequency and low-frequency components simultaneously with convolutional-residual Fourier layers and equivariant attentions in a hierarchical structure.
- The proposed method surpasses previous state-of-the-art approaches in existing PDE benchmarks, including Navier-Stokes equations, Darcy equations, and particularly multiscale elliptic equations with rapidly changing coefficients and significant solution variations.
- Furthermore, our method demonstrates effectiveness and robustness in solving inverse PDE problems, particularly when dealing with noisy input data.

### Related works

We briefly cover the background and related works in this section. More related works are listed in the Appendix.

#### Neural PDE solver

Many excellent algorithms have been proposed previously for solving PDEs using neural networks (Long et al. 2018; Hao et al. 2022). Physics-informed neural network (PINN) (Karniadakis et al. 2021) incorporates PDEs into the network by giving additional constraints with the form of PDEs into loss function, which then guide the synaptic modifications towards tuned parameters that satisfy data distribution, physical PDE laws, and other necessary boundary conditions. GT (Cao 2021) utilizes the self-attention mechanism to build operator learners to solve PDEs and designs Fourier-type and Galerkin-type attention with linear complexity to reduce the computation cost. Neural operators leverage the concept that the operator denotes the mapping between infinite input and output function spaces. DeepONet (Lu, Jin, and Karniadakis 2019) leverages the universal approximation theorem to derive a branch-trunk structure to form the operator in a polynomial regression way. Some other methods incorporate trained neural networks into conventional numerical solvers, to minimize numerical errors when dealing with coarse grids (Cuomo et al. 2022; Meng et al. 2020). Our approach is also built on the concept of FNO (Li et al. 2020, 2022), which utilizes Green’s function and directly approximates the kernel in the Frequency domain. We incorporate different Fourier features at different frequency scales, which as a result, reaches promising performance in solving complex PDEs (e.g., multiscale PDEs).

#### Multiscale PDEs

Multiscale PDEs have many applications, including forecasting atmospheric convection and ocean circulation, modeling the subsurface of flow pressures (Furman 2008; Huyakorn 2012), the deformation of elastic materials (Rivlin 1948; Merodio and Ogden 2003), and the electric potential of conductive materials (Sundnes, Lines, and Tveito 2005). Multiscale elliptic PDEs are classic examples of multiscale PDEs. Solving elliptic PDEs with smooth coefficients is a conventional problem that can be effectively addressed using FNO. However, when the coefficients become non-smooth and exhibit rapidly changing features, the values in the solution spaces can exhibit oscillations and high contrast ratios (Anonymous 2023). Another example is turbulent flow, which is modeled by the Navier-Stokes equation. This equation describes fluid dynamics and exhibits turbulent behavior at high Reynolds numbers. In turbulent flow, unsteady vortices interact, leading to complex dynamics. To solve these multiscale PDEs effectively, models must account for both global and local dynamics. Equations and more details about multiscale PDEs are presented in the Appendix.

#### Fourier Neural Operator

Fourier neural operator (FNO) (Li et al. 2020, 2022) draws inspiration from the conventional Green’s function method and directly optimizes the kernel within the Fourier frequency domain by utilizing the Fast Fourier Transform (FFT). This approach has been demonstrated to be an efficient means of reducing computational cost and performing global convolution. A notable advancement is that the operator kernel is directly trained in the frequency domain, whereby the network is theoretically independent of the training data resolution. Thus, FNO (Li et al. 2020, 2022) can deal with super-resolution problems and be trained on multiple PDEs.

FNO has laid the foundation for operator learning, inspiring several subsequent works in the field. Geo-FNO (Li et al. 2022) deforms the irregular grid into a latent space with a uniform grid to solve the limitation of FFT which could only be applied to rectangular domains. F-FNO (Tran et al. 2021) learns the kernel weights in a factorized way with separable spectral layers. G-FNO (Helwig et al. 2023) utilizes the symmetry groups in the Fourier kernel to learn equivalent representations and improve accuracy even under imperfect symmetries.

However, FNO ignores high-frequency components by default to learn a smooth representation of the input space, which results in poor performance when solving PDEs with rapidly changing coefficients (Liu, Xu, and Zhang 2022). To address this limitation, we integrate convolutional-residual Fourier layers and equivariant attention mechanisms to capture local and global frequency features simultaneously.

### Methods

In this section, we introduce our proposed method in detail. First, we formulate the definition of operator learning and illustrate FNO only learning the low-frequency domain. Then,

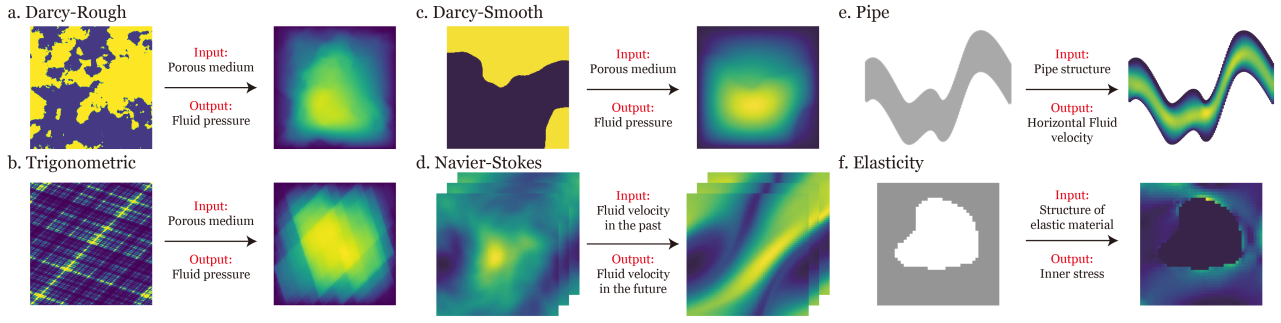


Figure 1: Examples of various tasks, including Darcy-Rough, Trigonometric, Darcy-Smooth, Navier-Stokes, Pipe, and Elasticity datasets. These datasets solve equations according to coefficients, previous solutions, and structures by approximating mappings between input and output in coordinate spaces. All these tasks are covered in experimental verification.

we theoretically prove the theorem to combine the attention mechanism and Fourier transformation in a translation-equivariant way. Finally, we introduce the architecture of our proposed model.

### Problem Formulation

For a PDE problem, the observed samples are  $(a_i, u_i)_{i=1}^N$ . Assuming the coordinates in a bounded open set  $\mathcal{D} \subset \mathbb{R}^d$ , both the input and output can be expressed as functions with respect to these coordinates. These functions belong to the Banach spaces  $\mathcal{X} = \mathcal{X}(\mathcal{D}; \mathbb{R}^{d_a})$  and  $\mathcal{Y} = \mathcal{Y}(\mathcal{D}; \mathbb{R}^{d_u})$  respectively. Here,  $\mathbb{R}^{d_a}$  and  $\mathbb{R}^{d_u}$  denotes the range of input and output functions.  $\mathcal{D}$  consists of a finite set of grid points within a rectangular area in  $\mathbb{R}^2$ . The function values are represented by position  $x \subset \mathcal{D}$ , which could be denoted as  $a(x)$  and  $u(x)$ . The overall solving process could be viewed as using a neural network  $f_\theta$  to approximate the mapping  $\mathcal{X} \rightarrow \mathcal{Y}$  to predict the output  $\hat{u}(x)$ , where  $\hat{u}(x) = f_\theta(a)(x)$ .

The Fourier neural operator (Li et al. 2020) is a powerful and efficient architecture for modeling PDEs that learn operators for mapping input and output function spaces. This algorithm is inspired by Green’s function method by learning the kernel integral operator defined below.

Define the kernel integral operator mapping by

$$[\mathcal{K}(\phi)a](x) = \int k_\phi(x, y)a(y)dy, \quad \forall x \in \mathcal{D}, \quad (1)$$

where Green’s function  $k_\phi$  is parameterized by neural networks with parameter  $\phi$ . In this context, the function  $k_\phi$  serves as a kernel function that is learned from data. FNO assumes that Green’s function is periodic and only dependent on the relative distance, which means that  $k_\phi(x, y) = k_\phi(x - y)$ . Then the operation in Eq. 1 could be regarded as convolution and efficiently implemented as element-wise multiplication in the frequency domain by using the convolution theorem:

$$\begin{aligned} [\mathcal{K}(\phi)a](x) &= \int k_\phi(x - y)a(y)dy \\ &= \mathcal{F}^{-1}(\mathcal{F}(k_\phi) \cdot \mathcal{F}(a))(x) \\ &= \mathcal{F}^{-1}(R_\phi \cdot \mathcal{F}(a))(x), \end{aligned} \quad (2)$$

where  $\mathcal{F}$  and  $\mathcal{F}^{-1}$  are the Fourier transform and the inverse Fourier transform, respectively. Instead of learning the kernel  $k_\phi$ , FNO directly learns the kernel  $R_\phi$  in the Fourier domain.

It is important to note that although the integral operator itself is linear, the neural operator can learn non-linear operators by using non-linear activation functions. Thus, the Fourier layer can be formally expressed as:

$$\hat{u}(x) := \sigma(Wa(x) + \mathcal{F}^{-1}(R_\phi \cdot \mathcal{F}(a))(x)), \quad \forall x \in \mathcal{D}, \quad (3)$$

where  $\sigma$  denotes the non-linear activation function,  $W$  and  $R_\phi$  are the fully connected layer and trainable operator kernel, respectively.

### FNO Drawbacks

Nevertheless, we take a one-dimensional case as an example to show that high-frequency features are not well represented in FNO and related methods, posing a challenge in dealing with multiscale PDEs. During the Fourier transformation process of the FNO, only the low-frequency components ( $\omega \leq T_\omega$ ) are reserved for multiplication, and high-frequency components ( $\omega > T_\omega$ ) are ignored by default. The size of the kernel is the same as the size of the reserved low-frequency components. Thus the elementwise multiplication process could be expressed as:

$$(R_\phi \cdot \mathcal{F}(a))(\omega) = \begin{cases} (R_\phi \cdot \mathcal{F}(a))(\omega), & \omega \leq T_\omega, \\ 0, & \omega > T_\omega. \end{cases}$$

Therefore, after inverse Fourier transformation,

$$\mathcal{F}^{-1}(R_\phi \cdot \mathcal{F}(a))(x) = \sum_{\omega \leq T_\omega} (R_\phi \cdot \mathcal{F}(a))(\omega)e^{i\omega x},$$

only the low-frequency components are represented. For the sake of notational convenience, we only use the one-dimensional case for illustration, which still stands for 2D and 3D cases. Additionally, previous works (Liu, Xu, and Zhang 2022) also inform that FNO and GT have shown their tendency to prioritize learning low-frequency components before high-frequency components when applied to multi-scale PDEs. Therefore, obtaining information about different input function frequencies is crucial to solving complex

PDEs. Motivated by the need to handle PDEs at multiple scales, this paper introduces a novel hierarchical attentive Fourier neural operator.

### Attentive Equivariant Convolution

In the FNO (Li et al. 2020), the kernel of Green’s function is imposed as the convolution kernel, which is a natural choice from the perspective of fundamental solutions. A fundamental property of the convolution is that it commutes with translations,

$$\mathcal{L}_y[f \star \psi](x) = [\mathcal{L}_y[f] \star \psi](x) \quad (4)$$

where  $L_y$  is the translation operator.<sup>1</sup> In other words, convolving a  $y$ -translated signal  $\mathcal{L}_y[f]$  with a filter is equivalent to first convolving the original signal  $f$  with the filter  $\psi$  and  $y$ -translating the obtained response next. This property is referred to as translation equivariance.

Previous works have defined attentive group convolution (Romero et al. 2020; Cohen and Welling 2016) and proved its equivariant property. We simplify them into attentive convolution defined on  $\mathbb{R}^d$ ,

$$[f \star^\alpha \psi](x) = \int_{\mathbb{R}^d} \alpha(x, \tilde{x}) f(\tilde{x}) \mathcal{L}_x[\psi](\tilde{x}) d\tilde{x} \quad (5)$$

where  $\alpha(x, \tilde{x})$  is the attention map between the input and output positions.

**Theorem 1.** *The attentive convolution is an equivariant operator if and only if the attention operator  $\mathcal{A}$  satisfies:*

$$\forall_{\tilde{x}, x, \tilde{x} \in \mathbb{R}^d} : \mathcal{A}[\mathcal{L}_{\tilde{x}} f](x, \tilde{x}) = \mathcal{A}[f](\tilde{x}^{-1}x, \tilde{x}^{-1}\tilde{x}) \quad (6)$$

*If, moreover, the maps generated by  $\mathcal{A}$  are invariant to one of its arguments, and, hence, exclusively attend to either the input or the output domain, then  $\mathcal{A}$  satisfies Equation (6) if it is equivariant and thus, based on convolutions.*

Since convolutions and pooling operations are translation equivariant, mostly visual attention mechanisms are translation equivariant as well (Romero et al. 2020). One special case is channel attention based on fully connected layers (a non-translation equivariant map) in SE-Nets (Hu, Shen, and Sun 2018). However, the input of the fully connected layers is obtained via global average pooling, which has shown that it is equivalent to a pointwise convolution (Romero et al. 2020). Therefore, attention here is translation equivariant (Cohen et al. 2018).

Furthermore, previous works broadly assumed that the maps in visual attention do not depend on the filters  $\psi$  and could be equivariantly factorized into spatial  $\alpha^x$  and channel  $\alpha^c$  components. Hence, the attention coefficient  $\alpha$  is the sole function of the input signal and becomes only dependent on  $x$  (Equation (5)).

$$[f \star^\alpha \psi] = [f^\alpha \star \psi] = [(\alpha f) \star \psi] = [(\alpha^x \alpha^c f) \star \psi] \quad (7)$$

In this way, the attention maps  $\alpha$  can be shifted to the input feature map  $f$ . Resultantly, the attentive convolution

<sup>1</sup>It follows that  $\mathcal{L}_g[f](x) = f(g^{-1}x) = f(x - y)$ , where  $g^{-1} = -y$  is the inverse of  $g$  in the translation group  $(\mathbb{R}^d, +)$  for  $g = y$ .

is reduced to a sequence of conventional convolutions and point-wise non-linearities (Thm. 1), which further reduces the computational cost of attention.

Inspired by GFNO (Helwig et al. 2023), we further utilize the following group Fourier transformation theorem to illustrate our Attentive Equivariant Fourier Neural Operator.

**Theorem 2.** *Given the orthogonal group  $O(d)$  acting on functions defined on  $\mathbb{R}^d$  by the map  $(g, f) \mapsto L_g f$  where  $(L_g f)(x) := f(g^{-1}x)$ , the group action commutes with the Fourier-transform, i.e.  $\mathcal{F} \circ L_g = L_g \circ \mathcal{F}$ .*

This theorem describes the equivariance of the Fourier transformation, which means applying a transformation from  $O(d)$  to a function in physical space equally applies the transformation to the Fourier transform of the function. Hence, based on Equation (3), our model could be generally built as

$$\hat{\mathbf{u}} := \text{MLP}(\sigma(\mathbf{W}\mathbf{a} + \mathcal{F}^{-1}(R_\phi \cdot \mathcal{F}(\alpha^x \alpha^c \mathbf{a})))), \quad (8)$$

to avoid confusion, we make the input  $\mathbf{a}$  and output  $\mathbf{u}$  in bold and omit  $\forall x \in \mathcal{D}$ . We further introduce the details and modify our model architecture to better learn the high-frequency feature in the next subsection.

### Model Architecture

We propose a hierarchical attentive Fourier neural operator combined with convolutional-residual layers and attention mechanisms to learn the function mapping at various resolutions.

**Convolutional-Residual Fourier layers:** Inspired by DCNO (Anonymous 2023), we propose the convolution-residual Fourier layers which are composed of two main components. In the first component, the input feature is transformed into the frequency domain by the Fast Fourier Transform (FFT) and directly learning an element-wise weight in the frequency domain. We follow the setting of FNO, only reserving lower-frequency components and training the kernel weights on them. This setting aims to learn a smooth mapping to avoid jagged curves in solution spaces. However, this setting may ignore some details about the solution space, especially in solving multiscale PDEs. Since convolution utilizes a much smaller kernel size than the Fourier transform allowing the kernel to capture locally detailed information, we replaced the fully connected residual layers with a convolution layer. This approach pertains to the high-frequency components that are neglected by the Fourier layer. To prevent confusion, we simplify the coordinates  $x$  and denote the input and output of the convolutional-residual Fourier layer at the  $k$ -th scale as  $v^k$  and  $\tilde{v}^k$  respectively. Thus, the Fourier layers could be modulated as:

$$\tilde{v}^k = \sigma(\text{Conv}(v^k) + \mathcal{F}^{-1}(R_\phi \cdot \mathcal{F}(v^k))), \quad (9)$$

where  $\sigma$  denotes the GELU activation,  $R_\phi$  represents the kernel weights in the Fourier domain that should be trained. Although the convolutional residual layers help to capture some high-frequency features, relying solely on this component is not enough to capture all detailed information. We also leverage attention mechanisms to enhance the extraction and integration of information.

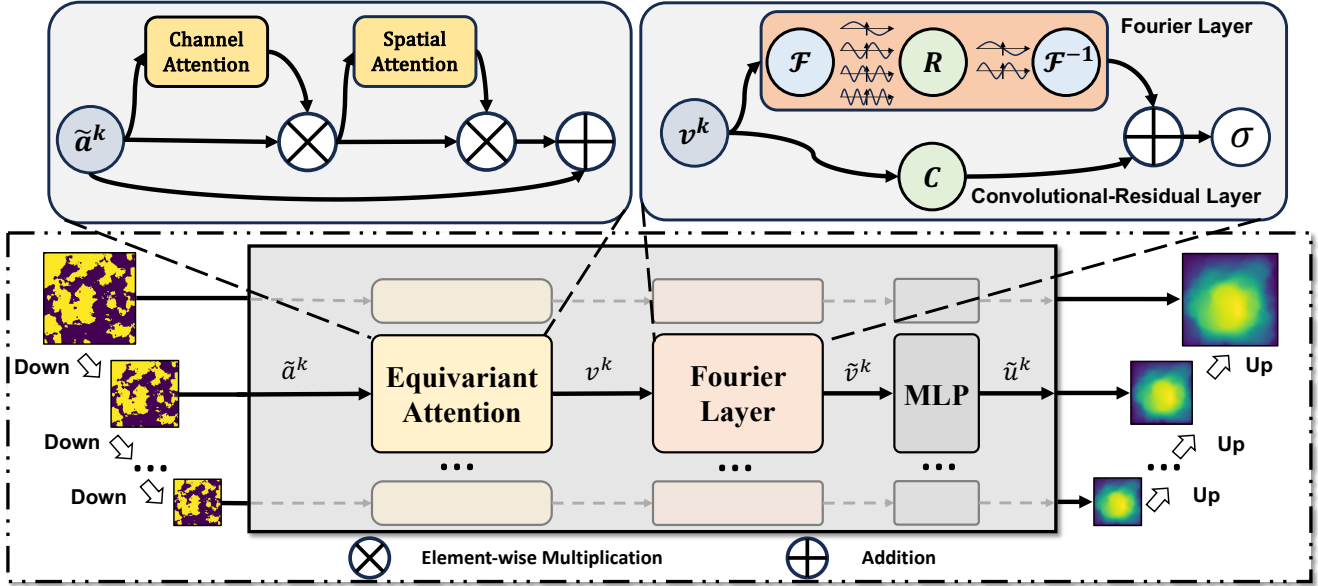


Figure 2: The overall network architecture. The input is downsampled and processed at each scale using equivariant attention and convolutional-residual Fourier layers. The final output is obtained by upsampling the outputs of hierarchical layers.

**Attention mechanism:** The attention mechanism can be regarded as a dynamic selection process, where it chooses important features while automatically disregarding irrelevant parts of the input features. The attention mechanism is suitable for learning dependence among pixels in the computer vision field (Yuan, Chen, and Wang 2020; Geng et al. 2021). Generally, the grid data in this work is similar to pixel images. Previous works have conducted thorough experiments to determine the optimal configuration for integrating channel and spatial attention maps in the  $\mathbb{R}^d$  scenario. We follow the settings in (Woo et al. 2018) that serially start with the channel attention.

$$\begin{aligned}
 \tilde{a}_c^k &= \mathcal{A}^c(\tilde{a}^k) \otimes \tilde{a}^k \\
 \tilde{a}_{xc}^k &= \mathcal{A}^x(\tilde{a}_c^k) \otimes \tilde{a}_c^k \\
 v^k &= \tilde{a}_{xc}^k + \tilde{a}^k
 \end{aligned} \tag{10}$$

where  $\tilde{a}^k$  serves as the input of the attention layers, which also denotes the downsampled feature of model input  $a$ .  $v^k$  represents the output of the attention layers.  $\otimes$  denotes the element-wise product. The  $\mathcal{A}^c$  and  $\mathcal{A}^x$  denote the channel and spatial attention respectively and have been proved to the equivariant operator before.

**Hierarchical architecture:** We attempt to design our model hierarchically, with various scales as inputs. As in multiscale PDEs, multiple scales and regions represent different physical laws (Karniadakis et al. 2021). The final prediction output is obtained by successively upsampling the outputs in various scales from coarse to fine. Specifically, for the  $k$ -scale,  $\tilde{u}^k$  is concatenated with the interpolation-upsampled  $\tilde{u}^{k+1}$  and further projected with a linear layer. More details are presented in the Appendix.

As the weight matrix is directly parameterized in the Fourier domain, we follow the FNO (Li et al. 2020) to limit

the Fourier series by terminating it at a predefined number of modes. In simple terms, we employ different truncation values at different hierarchical layers to ensure that our model can learn diverse information at different scales. However, large truncation modes would cause computing resources to increase hugely. To balance the computation cost and performance, we set the truncation mode to decrease with the feature scale, as we reckon that large-scale features need more Fourier modes to represent, detailed values are listed in the Appendix.

### Evaluation metrics

Previous works (Liu, Xu, and Zhang 2022; Anonymous 2023) proposed H1 loss to solve multiscale PDEs which calculates the loss in the Fourier domain. However, we only use the normalized mean squared error (N-MSE) as the loss function and evaluation metrics, which is defined as

$$\text{N-MSE} = \frac{1}{B} \sum_{i=1}^B \frac{\|\hat{u}_i - u_i\|_2}{\|\hat{u}_i\|_2}, \tag{11}$$

where  $\|\cdot\|_2$  is the 2-norm,  $B$  is the batch size,  $u$  and  $\hat{u}$  are the network output prediction and ground truth respectively.

### Experiments

**Benchmarks.** We evaluate our method on various PDE benchmarks, including multiscale elliptic equations with various resolutions, Navier-Stokes equations with different viscosity coefficients, and other physics scenarios governed by PDEs. Also, we conduct experiments on the inverse problem of multiscale elliptic equations with noise added to input data.

**Baselines.** We compare our method with recent and advanced methods. FNO (Li et al. 2020), U-NO (Rahman,

Table 1: Experiment results on various elliptic equations with various resolutions.  $\rightarrow$  denotes the resolution mapping between input and output. For example,  $256 \rightarrow 256$  denotes the input coefficient spaces are  $256 \times 256$  and the output solution spaces are  $256 \times 256$ . Performance is measured with mean squared error (MSE with  $\times 10^{-2}$ ). The number of parameters and time per epoch are measured for a batch size of 10. For clarity, the best result is in **bold** and the second best is underlined.

METHODS	PARAMETERS ( $\times 10^6$ )	TIME PER EPOCH (s)	TRIGONOMETRIC		DARCY ROUGH		DARCY-SMOOTH
			256 $\rightarrow$ 256	512 $\rightarrow$ 512	128 $\rightarrow$ 128	256 $\rightarrow$ 256	64 $\rightarrow$ 64
FNO	2.42	7.42	1.936	1.932	2.160	2.098	1.08
WMT	10.32	20.03	1.043	1.087	1.573	1.621	0.82
U-NO	16.39	15.42	1.256	1.245	1.368	1.332	1.13
GT	3.27	36.32	1.143	1.264	2.231	2.423	1.70
F-FNO	4.87	10.42	1.429	1.424	1.435	1.513	0.77
HANO	15.84	29.13	0.893	0.948	1.172	1.241	0.79
LSM	5.81	14.26	<u>0.832</u>	<u>0.782</u>	<b>1.036</b>	1.014	<u>0.65</u>
DCNO	2.27	11.73	1.056	1.209	1.276	<u>0.948</u>	<u>0.72</u>
OURS	5.36	10.81	<b>0.722</b>	<b>0.695</b>	<u>1.161</u>	<b>0.904</b>	<b>0.59</b>

Ross, and Azizzadenesheli 2022), and F-FNO (Tran et al. 2021) are FNO-relevant methods that use Fourier transformation to learn the operators directly in the frequency domain. WMT (Gupta, Xiao, and Bogdan 2021) learns the kernel projection onto fixed multiwavelet polynomial bases. GT (Cao 2021) modify the self-attention to Fourier-type and Galerkin-type attentions with linear complexities to solve the PDEs. HANO (Liu, Xu, and Zhang 2022) utilizes hierarchical attention to solve multiscale PDEs. LSM (Wu et al. 2023) solves the PDEs in the latent spectrum domain by decomposing latent features into basic operators.

### Complex Elliptic Equations

The elliptic equation datasets describe the flow of fluid through a porous medium, which are formulated by a second-order linear elliptic equation,

$$\begin{cases} -\nabla \cdot (a(x)\nabla u(x)) = f(x), & x \in D, \\ u(x) = 0, & x \in \partial D, \end{cases} \quad (12)$$

with rough coefficients and Dirichlet boundary. Our model aims to approximate an operator, which maps the input coefficient function to the corresponding output solution space. In contrast to previous works, the coefficient functions show a significant degree of smoothness, leading to correspondingly smooth solutions. We follow the setting in HANO (Liu, Xu, and Zhang 2022) and DCNO (Anonymous 2023) to change the conventional elliptic equations into multiscale cases by modifying coefficients to two-pharse rough ones (**Darcy-Rough**) or high-contrast trigonometric coefficients (**Trigonometric**). More details are denoted in the Appendix.

The original experiments of multiscale PDEs using coefficients with resolution  $1023 \times 1023$  to approximate the solution with resolution  $256 \times 256$  or  $512 \times 512$  in the trigonometric setting, which reduce the difficulties as larger inputs might contain more specific information. To enhance the difficulty, we modify the resolution of coefficients to the same as that of the output solution. We also follow the setting in (Li et al. 2020) and perform the original elliptic equation dataset (**Darcy-Smooth**) for comparison.

The experiment results are presented in Table 1, our model achieves the lowest error compared to other oper-

Table 2: Experiments on various Navier-Stokes equations and other physical scenarios including Elasticity, Darcy-Smooth, and Pipe. Performances are measured with MSE ( $\times 10^{-2}$ ). Also, the best result is in **bold** and the second best is underlined.

Methods	Navier-Stokes			Elasticity	Pipe
	$\nu = 10^{-3}$	$\nu = 10^{-4}$	$\nu = 10^{-5}$		
	$T_0 = 10s$ $T = 50s$	$T_0 = 10s$ $T = 30s$	$T_0 = 10s$ $T = 20s$		
FNO	1.28	8.34	19.82	5.08	0.67
WMT	1.01	11.35	15.41	5.20	0.77
U-NO	0.89	<b>5.72</b>	17.53	4.69	1.00
GT	1.12	-	26.84	16.81	0.98
F-FNO	0.92	6.02	17.98	4.72	0.59
HANO	0.98	6.18	18.47	4.75	0.70
LSM	<u>0.82</u>	6.12	<u>15.35</u>	4.08	<b>0.50</b>
Ours	<b>0.72</b>	<u>5.92</u>	<b>15.09</b>	<b>3.89</b>	<u>0.51</u>

ator baselines in most situations, especially in the elliptic equations with trigonometric coefficients. Our results indicate that cascade architecture models, such as FNO and DCNO, perform suboptimally in this setting, while hierarchical structures, such as U-NO, HANO, and LSM, perform relatively better. However, the amount of parameters and computations required by HANO and UNO are considerable, our model reduces the parameter quantity by using equivariant attention and convolutions and reaches better prediction performances. To better show the improvement of our model in solving multiscale PDEs, we visualize the prediction solution and error in Figure 5. Compared with FNO, our model achieves lower prediction error, especially in high-frequency components, which shows the improvements of our model to capture high-frequency features.

### Navier-Stokes Equation

We consider the 2D Navier-Stokes equation, a standard benchmark proposed in FNO (Li et al. 2020), in which the vorticity forms on the two-dimensional torus  $\mathbb{T}^2$ .

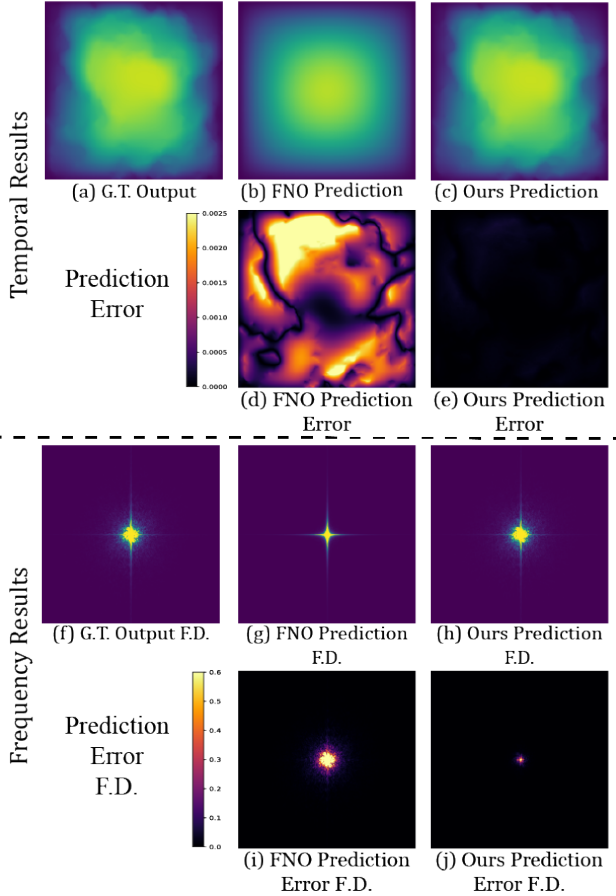


Figure 3: Showcase of Darcy-Rough Elliptic Equations, where the high-frequency components are moved to the center. **G.T.** and **F.D.** denote the ground truth and frequency domain. The absolute error is computed as  $|u - \hat{u}|$ .

Specifically, the operator predicts the vorticity after  $T_0$  by the input vorticity before  $T_0$ , the values of  $T_0$  and  $T$  vary according to the dataset. Our experiments consider viscosities with  $\nu \in \{10^{-3}, 10^{-4}, 10^{-5}\}$ , with smaller viscosities denoting more chaotic flow, are much harder to predict. The ‘rollout’ strategy is employed to predict vorticity at each time step in a recursive manner to ensure fair comparisons. The final operator could be regarded as approximated by various neural operators.

### Other physical scenarios

We further evaluate our method on Pipe and Elasticity datasets.

**Pipe:** The Pipe dataset focuses on predicting the incompressible flow through a pipe. The input is the pipe structure, while the output is the horizontal fluid velocity within the pipe. In this dataset, geometrically structured meshes with resolution  $129 \times 129$  are generated. The input and output are the mesh structure and fluid velocity within the pipe.

**Elasticity:** The Elasticity dataset is designed to predict the internal stress within an incompressible material containing an arbitrary void at its center and an external tensile force

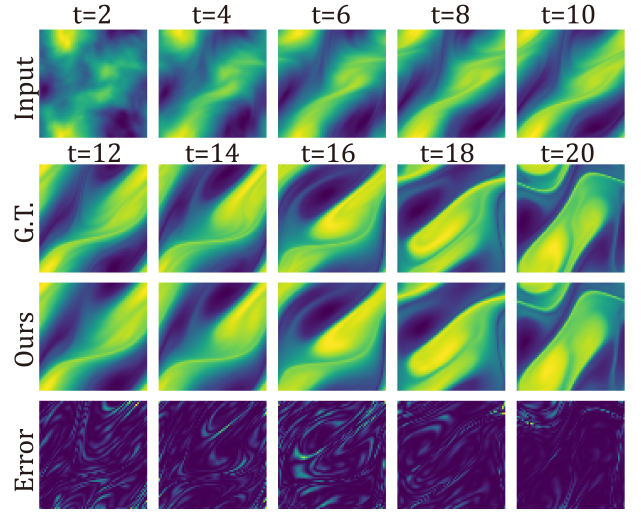


Figure 4: Showcase of prediction results and absolute error of our model in the Navier-Stokes equation dataset. First row:  $\{2, 4, 6, 8, 10\}$  time steps input sequence; Second row:  $\{12, 14, 16, 18, 20\}$  time steps ground truth sequence; Third row: corresponding prediction sequence; Last row: corresponding absolute prediction error  $|\hat{x} - y|$ .

is exerted on the material. Originally, the Elasticity data are presented by the point clouds, we follow (Wu et al. 2023) to modify the data into regular grids. The input consists of the material’s structural characteristics, while the output represents the internal stress. These benchmarks estimate the inner stress of incompressible materials with an arbitrary void in the center of the material. In addition, external tension is applied to the material. This benchmark’s input and output are the material’s structure and inner stress.

We evaluate our model on these datasets to demonstrate the effectiveness of our model in solving general PDE problems. Table 2 summarizes experimental results on Navier-Stokes equations with various coefficients and other physical scenarios. Our model performs better in almost all settings, especially in the Navier-Stokes dataset with small viscosities and Elasticity dataset. Learning high-frequency features may help capture detailed flow changes as flows with smaller viscosities are more chaotic.

Our experimental results demonstrate that our model reaches superior performance compared with LSM (Wu et al. 2023), the previous state-of-the-art approach, which utilizes a combination of self-attention and latent spectral decomposition to solve PDEs within the latent domain. Despite this, it is important to note that LSM is not an operator since it relies on patched multiscale architectures and self-attention mechanisms. We further visualize the results of Navier-Stokes in Figure 5.

### Inverse Problems Solving

In various scientific disciplines such as geological sciences and mathematical derivation, inverse problems are of significant importance. Nonetheless, these problems frequently demonstrate reduced stability compared to their associated

Table 3: Experiments on inverse coefficient identification tasks. In this experiment, the input solution space and output coefficient space are both  $256 \times 256$ . Performances are measured with MSE ( $\times 10^{-2}$ ). Also, the best result is in **bold** and the second best is underlined.

methods	Trigonometric			Darcy rough		
	$\epsilon = 0$	$\epsilon = 0.01$	$\epsilon = 0.1$	$\epsilon = 0$	$\epsilon = 0.01$	$\epsilon = 0.1$
FNO	44.74	46.34	48.43	28.41	28.98	30.65
WMT	11.14	<u>12.43</u>	20.43	12.32	17.54	28.43
U-NO	12.97	18.54	25.87	15.64	20.54	25.34
GT	27.87	30.98	43.54	23.12	28.87	35.43
F-FNO	21.46	26.98	36.34	18.73	25.23	37.54
HANO	9.87	13.67	20.98	8.45	<u>10.43</u>	<u>20.43</u>
DCNO	<u>8.87</u>	17.64	34.76	<b>6.32</b>	11.83	23.54
Ours	<b>8.32</b>	<b>10.14</b>	<b>18.24</b>	<u>7.48</u>	<b>9.42</b>	<b>17.32</b>

forward problems, even when advanced regularization techniques are employed.

Following (Anonymous 2023), we evaluate our method for inverse identification problems on multiscale elliptic PDEs. In this experiment, we aim to learn an inverse operator, which maps the solution function space to the corresponding coefficient space  $\hat{u} = u + \epsilon N(u) \mapsto a$ . Here,  $\epsilon$  indicates the extent of Gaussian noise introduced into the training and evaluation data. The noise term  $N(u)$  accounts for the sampling distribution and data-related noise.

The experiments about inverse coefficients inference problems on the multiscale elliptic PDEs dataset are presented in Table 3. In our experiments, we modify the input and output resolutions to both  $256 \times 256$  in the Darcy Rough and Trigonometric elliptic equations. Since the coefficient function space changes faster than the solution space, this task is more challenging than the forward-solving problem.

The result shows that our model performs well in the inverse coefficient identification problem, which illustrates our model’s ability to successfully address the challenges posed by this ill-posed inverse problem with data. Methods such as FNO and F-FNO that learn kernel functions directly in the low-frequency domain have trouble recovering targets with high-frequency components.

### Ablation study

To verify the effectiveness of each component in our model, we perform ablation studies in various settings, including removing components (*w/o*), replacing them with other components (*rep*), and adding some other components (*add*).

- In the *w/o* part, we consider removing the attention component (*w/o* Attention) or even the Fourier layer (*w/o* FNO).
- In the *rep* part, we consider replacing the convolutional-residual layer and attention mechanism with other components and keeping the number of parameters almost unchanged. For convolutional-residual layers, we replace them with simple residual layers (*rep* Conv→Res) or fully connected layers (*rep* Conv→Fc). For the attention mechanism, we replace them with dilation convo-

Table 4: Ablation studies on our proposed model, including removing components (*w/o*), replacing them with other components (*rep*), and adding some other components (*add*). Performances are measured with MSE ( $\times 10^{-2}$ ) and the best result is in **bold**.

Designs	MSE			
	Trigono	Darcy-Rough	Navier-Stokes	
<i>w/o</i>	Attention	1.054	1.162	17.25
	FNO	1.228	1.306	22.31
<i>rep</i>	Conv→Res	1.131	1.162	16.46
	Conv→Fc	1.176	1.245	15.72
	Att→d-Conv	0.894	0.954	16.12
	Att→MLP	0.985	1.034	15.63
<i>add</i>	Hier	0.794	<b>0.901</b>	15.36
<b>Ours</b>		<b>0.722</b>	0.904	<b>15.29</b>

lution (*rep* Att→d-Conv) or multi-layer perceptrons (*rep* Att→MLP).

- In the *add* part, we add one hierarchical layer with corresponding attention and Fourier layer (*add* Hier).

It is discovered that all components of our model are essential for solving multiscale PDEs after removing experiments. Without the attention and Fourier layer, model performance on all benchmarks will drop seriously. Similar results could be found in replacing experiments, the convolutional-residual Fourier layer and attention can fit the multiscale PDEs benchmarks well. Besides, in the Navier-Stokes dataset, MLP achieved performance comparable to attention, suggesting that previous methods can work well in PDEs where the coefficients do not change rapidly. Additionally, adding a hierarchical layer may improve the performance of the model sometimes, but this will add a significant amount of computation. To balance the efficiency and effectiveness we keep the number of layers of our model. Last but not least, our model performs better than methods with cascade architecture, such as FNO and F-FNO, indicating the importance of solving multiscale PDEs hierarchically.

### Conclusion

We propose a novel hierarchical attentive Fourier neural operator that combines convolutional-residual Fourier layers and equivariant attentions for solving multiscale PDEs. Our model utilizes Fourier layers to learn low-frequency features, with convolutional-residual layer and attention mechanisms to capture high-frequency features. Benefits from the above components, our model could capture both local and global information and achieve superior performances in many PDE benchmarks, especially in solving forward and inverse problems of multiscale elliptic PDEs.

Many works should be done in the future. Researching how to solve more complicated PDEs or even complex dynamics in the real scene and how to use the property of PDEs to design neural network architectures is meaningful.



## References

- Anonymous. 2023. Dilated convolution neural operator for multiscale partial differential equations. In *Submitted to The Twelfth International Conference on Learning Representations*. Under review.
- Brandstetter, J.; Berg, R. v. d.; Welling, M.; and Gupta, J. K. 2022. Clifford neural layers for PDE modeling. *arXiv preprint arXiv:2209.04934*.
- Cao, S. 2021. Choose a transformer: Fourier or galerkin. *Advances in neural information processing systems*, 34: 24924–24940.
- Chen, R. T.; Rubanova, Y.; Bettencourt, J.; and Duvenaud, D. K. 2018. Neural ordinary differential equations. *Advances in neural information processing systems*, 31.
- Cohen, T.; and Welling, M. 2016. Group equivariant convolutional networks. In *International conference on machine learning*, 2990–2999. PMLR.
- Cohen, T. S.; Geiger, M.; Köhler, J.; and Welling, M. 2018. Spherical cnns. *arXiv preprint arXiv:1801.10130*.
- Cuomo, S.; Di Cola, V. S.; Giampaolo, F.; Rozza, G.; Raissi, M.; and Piccialli, F. 2022. Scientific machine learning through physics-informed neural networks: Where we are and what’s next. *Journal of Scientific Computing*, 92(3): 88.
- Dai, J.; Qi, H.; Xiong, Y.; Li, Y.; Zhang, G.; Hu, H.; and Wei, Y. 2017. Deformable convolutional networks. In *Proceedings of the IEEE international conference on computer vision*, 764–773.
- Devlin, J.; Chang, M.-W.; Lee, K.; and Toutanova, K. 2018. Bert: Pre-training of deep bidirectional transformers for language understanding. *arXiv preprint arXiv:1810.04805*.
- Dong, L.; Xu, S.; and Xu, B. 2018. Speech-transformer: a no-recurrence sequence-to-sequence model for speech recognition. In *2018 IEEE international conference on acoustics, speech and signal processing (ICASSP)*, 5884–5888. IEEE.
- Engquist, B.; and Souganidis, P. E. 2008. Asymptotic and numerical homogenization. *Acta Numerica*, 17: 147–190.
- Furman, A. 2008. Modeling coupled surface–subsurface flow processes: a review. *Vadose Zone Journal*, 7(2): 741–756.
- Geng, Z.; Guo, M.-H.; Chen, H.; Li, X.; Wei, K.; and Lin, Z. 2021. Is attention better than matrix decomposition? *arXiv preprint arXiv:2109.04553*.
- Gopakumar, V.; Pamela, S.; Zanisi, L.; Li, Z.; Anandkumar, A.; and Team, M. 2023. Fourier Neural Operator for Plasma Modelling. *arXiv preprint arXiv:2302.06542*.
- Guibas, J.; Mardani, M.; Li, Z.; Tao, A.; Anandkumar, A.; and Catanzaro, B. 2021. Adaptive fourier neural operators: Efficient token mixers for transformers. *arXiv preprint arXiv:2111.13587*.
- Gulati, A.; Qin, J.; Chiu, C.-C.; Parmar, N.; Zhang, Y.; Yu, J.; Han, W.; Wang, S.; Zhang, Z.; Wu, Y.; et al. 2020. Conformer: Convolution-augmented transformer for speech recognition. *arXiv preprint arXiv:2005.08100*.
- Guo, M.-H.; Xu, T.-X.; Liu, J.-J.; Liu, Z.-N.; Jiang, P.-T.; Mu, T.-J.; Zhang, S.-H.; Martin, R. R.; Cheng, M.-M.; and Hu, S.-M. 2022. Attention mechanisms in computer vision: A survey. *Computational visual media*, 8(3): 331–368.
- Gupta, G.; Xiao, X.; and Bogdan, P. 2021. Multiwavelet-based operator learning for differential equations. *Advances in neural information processing systems*, 34: 24048–24062.
- Hackbusch, W. 2013. *Multi-grid methods and applications*, volume 4. Springer Science & Business Media.
- Hafner, D.; Lillcrap, T.; Ba, J.; and Norouzi, M. 2019. Dream to control: Learning behaviors by latent imagination. *arXiv preprint arXiv:1912.01603*.
- Hao, Z.; Liu, S.; Zhang, Y.; Ying, C.; Feng, Y.; Su, H.; and Zhu, J. 2022. Physics-informed machine learning: A survey on problems, methods and applications. *arXiv preprint arXiv:2211.08064*.
- Hao, Z.; Wang, Z.; Su, H.; Ying, C.; Dong, Y.; Liu, S.; Cheng, Z.; Song, J.; and Zhu, J. 2023. Gnot: A general neural operator transformer for operator learning. In *International Conference on Machine Learning*, 12556–12569. PMLR.
- He, K.; Zhang, X.; Ren, S.; and Sun, J. 2016. Deep residual learning for image recognition. In *Proceedings of the IEEE conference on computer vision and pattern recognition*, 770–778.
- Helwig, J.; Zhang, X.; Fu, C.; Kurtin, J.; Wojtowysch, S.; and Ji, S. 2023. Group Equivariant Fourier Neural Operators for Partial Differential Equations. *arXiv preprint arXiv:2306.05697*.
- Hu, H.; Gu, J.; Zhang, Z.; Dai, J.; and Wei, Y. 2018. Relation networks for object detection. In *Proceedings of the IEEE conference on computer vision and pattern recognition*, 3588–3597.
- Hu, J.; Shen, L.; and Sun, G. 2018. Squeeze-and-excitation networks. In *Proceedings of the IEEE conference on computer vision and pattern recognition*, 7132–7141.
- Huyakorn, P. S. 2012. *Computational methods in subsurface flow*. academic press.
- Karniadakis, G. E.; Kevrekidis, I. G.; Lu, L.; Perdikaris, P.; Wang, S.; and Yang, L. 2021. Physics-informed machine learning. *Nature Reviews Physics*, 3(6): 422–440.
- Li, Z.; Huang, D. Z.; Liu, B.; and Anandkumar, A. 2022. Fourier neural operator with learned deformations for pdes on general geometries. *arXiv preprint arXiv:2207.05209*.
- Li, Z.; Kovachki, N.; Azizzadenesheli, K.; Liu, B.; Bhattacharya, K.; Stuart, A.; and Anandkumar, A. 2020. Fourier neural operator for parametric partial differential equations. *arXiv preprint arXiv:2010.08895*.
- Li, Z.; Meidani, K.; and Farimani, A. B. 2022. Transformer for partial differential equations’ operator learning. *arXiv preprint arXiv:2205.13671*.
- Liu, S.; Hao, Z.; Ying, C.; Su, H.; Cheng, Z.; and Zhu, J. 2023. NUNO: A General Framework for Learning Parametric PDEs with Non-Uniform Data. *arXiv preprint arXiv:2305.18694*.
- Liu, X.; Xu, B.; and Zhang, L. 2022. Ht-net: Hierarchical transformer based operator learning model for multiscale pdes. *arXiv preprint arXiv:2210.10890*.
- Long, Z.; Lu, Y.; Ma, X.; and Dong, B. 2018. Pde-net: Learning pdes from data. In *International conference on machine learning*, 3208–3216. PMLR.
- Lu, L.; Jin, P.; and Karniadakis, G. E. 2019. DeepONet: Learning nonlinear operators for identifying differential equations based on the universal approximation theorem of operators. *arXiv preprint arXiv:1910.03193*.
- Meng, X.; Li, Z.; Zhang, D.; and Karniadakis, G. E. 2020. PPINN: Parareal physics-informed neural network for time-dependent PDEs. *Computer Methods in Applied Mechanics and Engineering*, 370: 113250.
- Merodio, J.; and Ogden, R. 2003. Instabilities and loss of ellipticity in fiber-reinforced compressible non-linearly elastic solids under plane deformation. *International Journal of Solids and Structures*, 40(18): 4707–4727.
- Ovadia, O.; Kahana, A.; Stinis, P.; Turkel, E.; and Karniadakis, G. E. 2023a. ViTO: Vision Transformer-Operator. *arXiv preprint arXiv:2303.08891*.
- Ovadia, O.; Turkel, E.; Kahana, A.; and Karniadakis, G. E. 2023b. DiTTO: Diffusion-inspired Temporal Transformer Operator. *arXiv preprint arXiv:2307.09072*.

- Owhadi, H. 2017. Multigrid with rough coefficients and multiresolution operator decomposition from hierarchical information games. *Siam Review*, 59(1): 99–149.
- Park, J.; Woo, S.; Lee, J.-Y.; and Kweon, I. S. 2018. Bam: Bottle-neck attention module. *arXiv preprint arXiv:1807.06514*.
- Pathak, J.; Subramanian, S.; Harrington, P.; Raja, S.; Chattopadhyay, A.; Mardani, M.; Kurth, T.; Hall, D.; Li, Z.; Azizzadenesheli, K.; et al. 2022. Fourcastnet: A global data-driven high-resolution weather model using adaptive fourier neural operators. *arXiv preprint arXiv:2202.11214*.
- Quarteroni, A.; and Veneziani, A. 2003. Analysis of a geometrical multiscale model based on the coupling of ODE and PDE for blood flow simulations. *Multiscale Modeling & Simulation*, 1(2): 173–195.
- Rahman, M. A.; Ross, Z. E.; and Azizzadenesheli, K. 2022. U-no: U-shaped neural operators. *arXiv preprint arXiv:2204.11127*.
- Rao, Y.; Zhao, W.; Zhu, Z.; Lu, J.; and Zhou, J. 2021. Global filter networks for image classification. *Advances in neural information processing systems*, 34: 980–993.
- Rivlin, R. 1948. Large elastic deformations of isotropic materials. I. Fundamental concepts. *Philosophical Transactions of the Royal Society of London. Series A, Mathematical and Physical Sciences*, 240(822): 459–490.
- Romero, D.; Bekkers, E.; Tomczak, J.; and Hoogendoorn, M. 2020. Attentive group equivariant convolutional networks. In *International Conference on Machine Learning*, 8188–8199. PMLR.
- Sommerfeld, A. 1949. *Partial differential equations in physics*. Academic press.
- Sundnes, J.; Lines, G. T.; and Tveito, A. 2005. An operator splitting method for solving the bidomain equations coupled to a volume conductor model for the torso. *Mathematical biosciences*, 194(2): 233–248.
- Tran, A.; Mathews, A.; Xie, L.; and Ong, C. S. 2021. Factorized fourier neural operators. *arXiv preprint arXiv:2111.13802*.
- Woo, S.; Park, J.; Lee, J.-Y.; and Kweon, I. S. 2018. Cbam: Convolutional block attention module. In *Proceedings of the European conference on computer vision (ECCV)*, 3–19.
- Wu, H.; Hu, T.; Luo, H.; Wang, J.; and Long, M. 2023. Solving High-Dimensional PDEs with Latent Spectral Models. *arXiv preprint arXiv:2301.12664*.
- Xu, J.; and Zikatanov, L. 2017. Algebraic multigrid methods. *Acta Numerica*, 26: 591–721.
- Yuan, Y.; Chen, X.; and Wang, J. 2020. Object-contextual representations for semantic segmentation. In *Computer Vision—ECCV 2020: 16th European Conference, Glasgow, UK, August 23–28, 2020, Proceedings, Part VI 16*, 173–190. Springer.
- Zhang, T.; Cheng, X.; Jia, S.; Li, C. T.; Poo, M.-m.; and Xu, B. 2023. A brain-inspired algorithm that mitigates catastrophic forgetting of artificial and spiking neural networks with low computational cost. *Science Advances*, 9(34): eadi2947.
- Zhao, X.; Sun, Y.; Zhang, T.; and Xu, B. 2024a. Enhanced Spatiotemporal Prediction Using Physical-guided And Frequency-enhanced Recurrent Neural Networks. *arXiv preprint arXiv:2405.14504*.
- Zhao, X.; Zhang, D.; Liyuan, H.; Zhang, T.; and Xu, B. 2024b. ODE-based Recurrent Model-free Reinforcement Learning for POMDPs. *Advances in Neural Information Processing Systems*, 36.
- Zhou, P.; Shi, W.; Tian, J.; Qi, Z.; Li, B.; Hao, H.; and Xu, B. 2016. Attention-based bidirectional long short-term memory networks for relation classification. In *Proceedings of the 54th annual meeting of the association for computational linguistics (volume 2: Short papers)*, 207–212.
- Zhou, T.; Ma, Z.; Wen, Q.; Wang, X.; Sun, L.; and Jin, R. 2022. Fedformer: Frequency enhanced decomposed transformer for long-term series forecasting. In *International Conference on Machine Learning*, 27268–27286. PMLR.

## Benchmark Details

We introduce the underlying PDEs of each benchmark and the number of corresponding training and testing samples.

### Multiscale Elliptic PDEs

Multiscale elliptic equations are given by second-order linear elliptic equations,

$$\begin{cases} -\nabla \cdot (a(x)\nabla u(x)) = f(x) & x \in D \\ u(x) = 0 & x \in \partial D \end{cases} \quad (13)$$

where the coefficient  $a(x) \in [a_{\min}, a_{\max}]$ ,  $\forall x \in D$  and  $a_{\min} > 0$ . The coefficient  $a(x)$ , enables rapid oscillation (for example, with  $a(x) = a(x/\varepsilon)$  where  $\varepsilon \ll 1$ ), a significant contrast ratio characterized by  $a_{\max}/a_{\min} \gg 1$ , and even a continuum of non-separable scales.

**Multiscale Trigonometric Coefficient** We follow the setting in HANO (Liu, Xu, and Zhang 2022), which considers eq. (13) with multiscale trigonometric coefficients. The domain  $D$  is  $[-1, 1]^2$ , and the coefficient  $a(x)$  is defined as

$$a(x) = \prod_{k=1}^6 (1 + \frac{1}{2} \cos(a_k \pi (x_1 + x_2))) (1 + \frac{1}{2} \sin(a_k \pi (x_2 - 3x_1))),$$

where  $a_k$  is uniformly distributed between  $2^{k-1}$  and  $1.5 \times 2^{k-1}$ , and the forcing term is fixed as  $f(x) \equiv 1$ . The resolution of the dataset is  $1023 \times 1023$  and lower resolutions are created by downsampling with linear interpolation.

**Two-Phase Coefficient** The two-phase coefficients and solutions are generated according to FNO (Li et al. 2020). The coefficients  $a(x)$  are generated according to  $a \sim \mu := \psi_{\#} \mathcal{N}(0, (-\Delta + cI)^{-2})$  with zero Neumann boundary conditions on the Laplacian. The mapping  $\psi : \mathbb{R} \rightarrow \mathbb{R}$  assigns the value  $a_{\max}$  to the positive segment of the real line and  $a_{\min}$  to the negative segment. The push-forward is explicitly defined on a pointwise basis. The forcing term is fixed as  $f(x) \equiv 1$ . The solutions  $u$  are derived through the application of a second-order finite difference approach on a well-suited grid. The parameters  $a_{\max}$  and  $a_{\min}$  have the ability to manage the contrast of the coefficient. Additionally, the parameter  $c$  regulates the roughness or oscillation of the coefficient; an increased value of  $c$  leads to a coefficient featuring rougher two-phase interfaces.

### Navier-Stokes

We follow the Navier-Stokes equation in FNO (Li et al. 2020). This dataset simulates incompressible and viscous flow on the unit torus, where fluid density is unchangeable. In this situation, energy conservation is independent of mass and momentum conservation.

$$\begin{aligned} \nabla \cdot u &= 0 \\ \frac{\partial w}{\partial t} + u \cdot \nabla w &= \nu \nabla^2 w + f \end{aligned} \quad (14)$$

$$w|_{t=0} = w_0,$$

where  $u$  and  $w$  are abbreviated versions of  $u(x, t)$  and  $w(x, t)$ , respectively.  $u \in \mathbb{R}^2$  is a velocity vector in 2D field,  $w = \nabla \times u$  is the vorticity,  $w_0 \in \mathbb{R}$  is the initial vorticity at  $t = 0$ . In this dataset, viscosity is set as

Table 5: More details about PDEs benchmarks, including the number of training and testing samples with their resolutions. NS is short for Navier-Stokes.

Benchmarks	$N_{training}$	$N_{testing}$	Resolution
Trigonometric	1000	100	$512 \times 512, 256 \times 256$
Darcy-Rough	1000	100	$256 \times 256, 128 \times 128$
Darcy-Smooth	1000	200	$64 \times 64$
NS( $\nu = 10^{-3}$ )	1000	200	$64 \times 64$
NS( $\nu = 10^{-4}$ )	10000	2000	$64 \times 64$
NS( $\nu = 10^{-5}$ )	1000	200	$64 \times 64$
Elasticity	1000	200	$41 \times 41$
Pipe	1000	200	$129 \times 129$

$\nu \in \{10^{-3}, 10^{-4}, 10^{-5}, 10^{-6}\}$  and the resolution of the 2D field is  $64 \times 64$ . The number of training and prediction frames is varied in different settings.

### Elasticity

The governing equation of Elasticity materials is:

$$\rho^s \frac{\partial^2 \mathbf{u}}{\partial t^2} + \nabla \cdot \boldsymbol{\sigma} = 0, \quad (15)$$

where  $\rho^s \in \mathbb{R}$  denotes the solid density,  $\nabla$  and  $\boldsymbol{\sigma}$  denote the nabla operator and the stress tensor respectively. Function  $\mathbf{u}$  represents the displacement vector of material over time  $t$ . These benchmarks estimate the inner stress of incompressible materials with an arbitrary void in the center of the material. In addition, external tension is applied to the material. This benchmark’s input and output are the material’s structure and inner stress.

### Pipe

This dataset focuses on the incompressible flow through a pipe. The governing equations are similar to Navier-Stokes equations:

$$\begin{aligned} \nabla \cdot \mathbf{U} &= 0 \\ \frac{\partial \mathbf{U}}{\partial t} + \mathbf{U} \cdot \nabla \mathbf{U} &= \mathbf{f} - \frac{1}{\rho} \nabla p + \nu \nabla^2 \mathbf{U}. \end{aligned} \quad (16)$$

In this dataset, geometrically structured meshes with resolution  $129 \times 129$  are generated. The input and output are the mesh structure and fluid velocity within the pipe.

We provide details of our benchmarks including the number of training and testing samples and their input solutions in table 5.

## Backgrounds and Proofs

### Proofs of Equivariant of Attentive Convolution

We follow the definition of (Cohen and Welling 2016) to define the attentive convolution and reduce the visual self-attention into

$$f_c^{out}(g) = \sum_{\tilde{c}} \int_G \alpha_{c, \tilde{c}}(g, \tilde{g}) \psi_{c, \tilde{c}}(g^{-1} \tilde{g}) f_{\tilde{c}}^{in}(\tilde{g}) d\tilde{g}. \quad (17)$$

In this work, we only consider group act on  $O(d)$ , thus the definition could be further reduced into

$$f_c^{out}(x) = \sum_{\tilde{c}}^{N_{\tilde{c}}} \int_{\mathbb{R}^d} \alpha_{c,\tilde{c}}(x, \tilde{x}) \psi_{c,\tilde{c}}(x^{-1}\tilde{x}) f_{\tilde{c}}^{in}(\tilde{x}) d\tilde{x}. \quad (18)$$

Without loss of generality, let  $\mathfrak{A} : \mathbb{L}_2(\mathbb{R}^d) \rightarrow \mathbb{L}_2(\mathbb{R}^d)$  denote the attentive group convolution defined by Equation (18), with  $N_{\tilde{c}} = N_c = 1$ , and some  $\psi$  which in the following we omit to simplify our derivation. Equivariance of  $\mathfrak{A}$  implies that  $\forall_{f \in \mathbb{L}_2(\mathbb{R}^d)}, \forall_{\tilde{x}, x \in \mathbb{R}^d}$ :

$$\begin{aligned} \mathfrak{A}[\mathcal{L}_{\tilde{x}}[f]](x) &= \mathcal{L}_{\tilde{x}}[\mathfrak{A}[f]](x) \\ &\Leftrightarrow \\ \mathfrak{A}[\mathcal{L}_{\tilde{x}}[f]](x) &= \mathfrak{A}[f](\tilde{x}^{-1}x) \\ &\Leftrightarrow \\ \int_{\mathbb{R}^d} \mathcal{A}[\mathcal{L}_{\tilde{x}}[f]](x, \tilde{x}) \mathcal{L}_{\tilde{x}}[f](\tilde{x}) d\tilde{x} &= \\ &= \int_{\mathbb{R}^d} \mathcal{A}[f](\tilde{x}^{-1}x, \tilde{x}) f(\tilde{x}) d\tilde{x} \\ &\Leftrightarrow \\ \int_{\mathbb{R}^d} \mathcal{A}[\mathcal{L}_{\tilde{x}}[f]](x, \tilde{x}) f(\tilde{x}^{-1}\tilde{x}) d\tilde{x} &= \\ &= \int_{\mathbb{R}^d} \mathcal{A}[f](\tilde{x}^{-1}x, \tilde{x}^{-1}\tilde{x}) f(\tilde{x}^{-1}\tilde{x}) d\tilde{x}, \end{aligned} \quad (19)$$

where we once again perform the variable substitution  $\tilde{x} \rightarrow \tilde{x}^{-1}\tilde{x}$  at the right hand side of the last step. This must hold for all  $f \in \mathbb{L}_2(\mathbb{R}^d)$  and hence:

$$\forall_{\tilde{x} \in \mathbb{R}^d} : \mathcal{A}[\mathcal{L}_{\tilde{x}}f](x, \tilde{x}) = \mathcal{A}[f](\tilde{x}^{-1}x, \tilde{x}^{-1}\tilde{x}) \quad (20)$$

### Proof of Symmetry of Fourier transform to $O(d)$

Let  $A \in \mathbb{R}^{d \times d}$  be an invertible matrix,  $f : \mathbb{R}^d \rightarrow \mathbb{R}$  Lebesgue-integrable and  $b \in \mathbb{R}^d$ . Consider the function  $f_{A,b} : \mathbb{R}^d \rightarrow \mathbb{R}$  given by  $f_{A,b}(x) = f(Ax + b)$ . Then

$$\mathcal{F}(f_{(A,b)})(\xi) = \frac{e^{-2\pi i \langle A^{-T}\xi, b \rangle}}{|\det A|} \mathcal{F}(f)(A^{-T}\xi)$$

In particular, if  $A$  is an orthogonal matrix, then  $|\det A| = 1$  and  $A^{-T} = A$ , so for all  $O \in O(n)$ :

$$\mathcal{F}(f_{(O,b)})(\xi) = e^{-2\pi i \langle O\xi, b \rangle} \mathcal{F}(f)(O\xi)$$

We will use the multi-dimensional change of variables formula with the substitution  $z = Ax + b$ , as well as the

Table 6: Model configurations.

MODEL DESIGNS	HYPERPARAMETERS	VALUES
FOURIER LAYERS	LOW-FREQUENCY MODES $\{d_{low}^1, \dots, d_{low}^K\}$	$\{24, 12, 6, 3\}$
HIERARCHICAL LAYERS	CHANNELS OF EACH SCALE $\{d_C^1, \dots, d_C^K\}$	$\{32, 64, 128, 128\}$
	NUMBER OF SCALES $K$	4
	DOWNSMAPLE RATIO $r$	2
TRAINING SETTING	LEARNING RATE BATCHSIZE	0.0005 10

identity  $\langle \xi, Az \rangle = \langle A^T \xi, z \rangle$ .

$$\begin{aligned} \mathcal{F}(f_{(A,b)})(\xi) &= \frac{1}{(2\pi)^{n/2}} \int_{\mathbb{R}^d} e^{-2\pi i \langle \xi, x \rangle} f_{(A,b)}(x) dx \\ &= \frac{1}{(2\pi)^{n/2} |\det A|} \int_{\mathbb{R}^d} e^{-2\pi i \langle \xi, A^{-1}(Ax+b) \rangle + 2\pi i \langle \xi, A^{-1}b \rangle} \\ &= \frac{1}{(2\pi)^{n/2} |\det A|} \int_{\mathbb{R}^d} e^{-2\pi i \langle \xi, A^{-1}z \rangle} f(z) dz \\ &= e^{2\pi i \langle \xi, A^{-1}b \rangle} \frac{1}{(2\pi)^{n/2} |\det A|} \int_{\mathbb{R}^d} e^{-2\pi i \langle \xi, A^{-1}z \rangle} f(z) dz \\ &= \frac{e^{2\pi i \langle \xi, A^{-1}b \rangle}}{|\det A|} \frac{1}{(2\pi)^{n/2}} \int_{\mathbb{R}^d} e^{-2\pi i \langle A^{-T}\xi, z \rangle} f(z) dz \\ &= \frac{e^{2\pi i \langle A^{-T}\xi, b \rangle}}{|\det A|} \mathcal{F}(f)(A^{-T}\xi). \end{aligned} \quad (21)$$

## Model Details

### Implementation Details.

Our model is implemented in PyTorch and conducted on a single NVIDIA A100 40GB GPU. Here are the implementation details of our model.

### Model Configurations.

Here we present the detailed model configurations of our model in table 6. In the beginning, the input data will be padded with zeros properly to resolve the division problem in model configurations.

### Downsample and Upsample Architecture

In this section, we illustrate the downsampling and upsampling operations in our hierarchical architectures. Our method is similar to that of LSM (Wu et al. 2023).

**Downsampling.** Given deep features  $\{\tilde{a}^k(x)\}_{x \in \mathcal{D}^k}$  at the  $k$ -th scale, The downsampling operation is to aggregate deep features in a local region through maximum pooling and convolution operations, which can be formalized as:

$$\begin{aligned} \{\tilde{a}^{k+1}(x)\}_{x \in \mathcal{D}^{k+1}} &= \text{Conv} \left( \text{MaxPool} \left( \{\tilde{a}^k(x)\}_{x \in \mathcal{D}^k} \right) \right), \\ & \quad k \text{ from } 1 \text{ to } (K-1). \end{aligned} \quad (22)$$

**Upsampling.** Given the features  $\tilde{u}^{k+1}(x)_{x \in \mathcal{D}^{k+1}}$  and  $\tilde{u}^k(x)_{x \in \mathcal{D}^k}$  corresponding to the  $(k+1)$ -th and  $k$ -th scales, respectively, the upsampling procedure involves fusing the interpolated features from the  $(k+1)$ -th scale and the features from the  $k$ -th scale using local convolution. This process can be expressed as follows:

$$\{\hat{u}^k(x)\}_{x \in \mathcal{D}^k} = \text{Conv} \left( \text{Concat} \left( \left[ \text{Interp} \left( \{\tilde{u}^{k+1}(x)\}_{x \in \mathcal{D}^{k+1}}, \{\tilde{u}^k(x)\}_{x \in \mathcal{D}^k} \right) \right] \right), \right. \\ \left. k \text{ from } (K-1) \text{ to } 1, \right) \quad (23)$$

where we adopt the bilinear Interpolation  $\text{Inter}(\cdot)$  for 2D data.

## More Related Work

### Operator Learning

Suppose  $\mathcal{A}$  and  $\mathcal{U}$  denote the infinite input and output function spaces. The objective of the operator is to learn a mapping from  $\mathcal{A}$  to  $\mathcal{U}$  using a finite collection of input and output pairs in the supervised learning way. For any vector function  $a \in \mathcal{A}$ ,  $a : \mathcal{D}_{\mathcal{A}} \rightarrow \mathbb{R}^{d_{\mathcal{A}}}$  with  $\mathcal{D}_{\mathcal{A}} \subset \mathbb{R}^d$  and for any vector function  $u \in \mathcal{U}$ ,  $u : \mathcal{D}_{\mathcal{U}} \rightarrow \mathbb{R}^{d_{\mathcal{U}}}$ , with  $\mathcal{D}_{\mathcal{U}} \subset \mathbb{R}^d$ . Given the training data  $\{(a_i, u_i)\}_{i=1}^N$ , our objective is to train an operator  $G_{\theta} : \mathcal{A} \rightarrow \mathcal{U}$  which is parameterized by  $\theta$ , to learn the mapping between input and output function spaces by extracting relationships from  $a$  and  $u$ .

### Numerical Solvers for Multiscale PDEs

In addressing multiscale PDEs, a variety of numerical approaches are available. Numerical homogenization methods (Engquist and Souganidis 2008) aim to create a finite-dimensional approximation space for solution exploration. Fast solvers like multilevel and multigrid methods (Hackbusch 2013; Xu and Zikatanov 2017) can be considered as an extension of numerical homogenization. Recently, operator-adapted wavelet methods, such as Gamblets (Owhadi 2017), have been developed to solve linear PDEs with rough coefficients, representing a progression beyond numerical homogenization. Nevertheless, handling multiscale PDEs poses inherent challenges for numerical methods, given that the computational cost tends to scale inversely proportional to the finest scale  $\epsilon$  of the problem. In recent years, there has been increasing exploration of neural network methods for solving multiscale PDEs (Anonymous 2023; Liu, Xu, and Zhang 2022).

### More FNO Related Work

Networks inspired by FNO have been verified in various domains, including computer vision and time series forecasting (Ovadia et al. 2023a,b). AFNO (Guibas et al. 2021) leverages kernel in the Fourier domain as a token mixer within the transformer, aiming at reducing computational complexity and enhancing performance in segmentation tasks. FED-former (Zhou et al. 2022) harnesses sparse basic elements

in the Fourier frequency domain to create a frequency-enhanced transformer. Meanwhile, GFNet (Rao et al. 2021) employs the element-wise multiplication of learnable global filters with features in the frequency domain to improve the performance in classification and transfer learning tasks.

### Visual Attention Methods

The attention mechanism can be regarded as a process of adaptive selection based on input features. It has yielded advantages in numerous visual tasks, including image classification (Woo et al. 2018), object detection (Dai et al. 2017; Hu et al. 2018), and semantic segmentation (Yuan, Chen, and Wang 2020; Geng et al. 2021). In computer vision, the attention mechanism is usually be divided into three main categories: channel attention, spatial attention, and temporal attention. For instance, SENet (Hu, Shen, and Sun 2018) utilizes global average pooling on the channel dimension to modulate the corresponding channel attention. Complementary channel attention akin to that of CBAM (Woo et al. 2018) and BAM (Park et al. 2018) utilize similar strategies for spatial attention and combine spatial and channel attention in series and parallel respectively. Recent research in visual attention aims to integrate the strengths of various attention mechanisms to create more holistic attention (Hu, Shen, and Sun 2018; Guo et al. 2022).

### More Visualization Results

We visualize more results on the Trigonometric dataset compared to FNO.

### Trigonometric

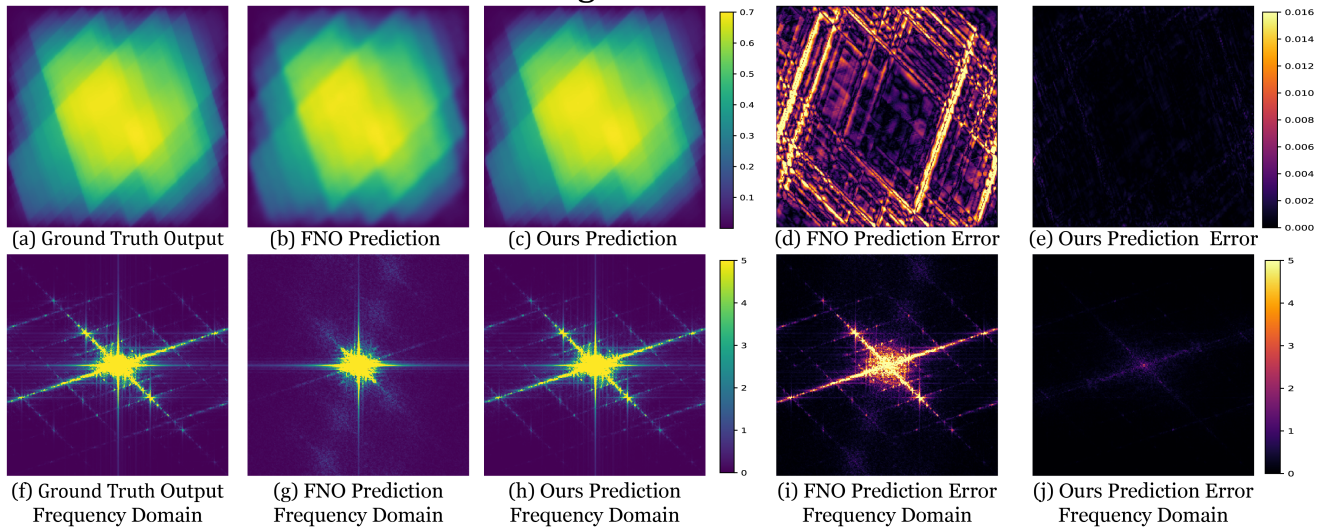


Figure 5: Showcase of multiscale PDEs, where the high-frequency components are moved to the center. **G.T.** and **F.D.** denote the ground truth and frequency domain. The absolute error is computed as  $|u - \hat{u}|$ .